Detection of Ar−HI by (2+1) REMPI

Toshinori Suzuki, Hideki Katayanagi, and Michael C. Heaven*

Institute for Molecular Science, Myodaiji, Okazaki 444, Japan

Received: March 3, 1997; In Final Form: April 25, 1997[⊗]

ArHI was detected by spectroscopic means for the first time. Analysis of the $g^3\Sigma^-(0^+)-X^1\Sigma^+(0^+)$ band system yielded estimates for the van der Waals bond strengths in the *g* and *X* states. The implications of these results for studies of the one-atom cage effect in RgHX complexes are considered.

Introduction

Rare-gas hydrogen halide complexes (Rg−HX) have proved to be excellent prototypes for investigations of intermolecular forces.[1−11] Ar−HX complexes are particularly well studied. Their ground states have been examined using microwave, far-IR, and IR techniques. Accurate intermolecular potential energy surfaces have been derived from the spectroscopic data for Ar−HF,[6,9] Ar−HCl,[1,7] and Ar−HBr.[1,8] For all three species, the potential surfaces have the same general features. The equilibrium geometry is linear Ar−HX, but there is also a second (shallower) minimum for linear HX−Ar.

Given the linear equilibrium geometry and favorable mass ratio combinations, Gerber and co-workers[12−16] have suggested that Rg−HX complexes may be suitable systems for exploring the one-atom cage effect. Photolysis of the H−X bond within the complex (via the repulsive $A\ ^1\Pi$ state) could result in trapped trajectories where the H atom chatters between the heavy atoms before escaping. Gerber et al.[12−16] predicted that the signature of these trapped trajectories should be observable in the H atom kinetic energy distribution. Subsequently, Segall et al.[15] have obtained results that were interpreted in terms of the one-atom cage effect in Ar−HBr. Photolysis of complexes in an expanding mixture of Ar/HBr yielded H atom kinetic energy distributions that were consistent with some loss of energy through collisions. However, there was some ambiguity in these results. The expanding gas mixture contained small amounts of Ar_n−HBr ($n > 1$) clusters and $(HBr)_2$ dimers. Segall et al.[15] were careful to note that the lower energy H atoms could have originated from these species.

As it is a difficult matter to generate a mass-selected beam of neutral clusters, development of a method for observing the dynamics of a specific species would be of value for future investigations of the cage effect in Rg−HX complexes. One way of doing this relies on the prediction that trapped trajectories (resonances) will produce broad structures in the continuum absorption spectra.[17] With a sensitive spectroscopic technique to monitor the concentration of ground-state complexes, a depletion technique could be employed to record a species-specific absorption spectrum.[18] (2+1) Resonance enhanced multiphoton ionization ((2+1) REMPI) detection of the complexes has the required sensitivity for this type of experiment. In addition, (2+1) REMPI is easily combined with time-of-flight mass spectrometry, to ensure detection of a single species. (2+1) REMPI spectra have been obtained for the HX monomers,[19−21] but so far there have been no reports of (2+1) REMPI spectra for Rg−HX complexes. In part, these considerations motivated the present search for the (2+1) REMPI spectrum of Ar−HI. This complex may be a good candidate for a depletion experiment, as the $A-X$ continuum lies in a convenient spectral region. However, the equilibrium geometry of the complex is not known and may not be favorable. Consequently, we were also interested in characterizing this species as it has not been observed previously by any spectroscopic means (other than mass spectroscopy).

Experimental Section

Ar−HI complexes were formed by supersonic expansion of a mixture of 2% HI in Ar. This mixture was expanded through a pulsed valve (0.8 mm orifice diameter) from a source pressure of 1800 Torr. The central region of the expanding gas was skimmed and directed through the extraction region of a time-of-flight mass spectrometer. Pulses from a tunable dye laser were used to ionize HI and Ar−HI. The wavelength drive of the laser was calibrated using a wavemeter (Burleigh Instruments). Frequency doubling was used to generate light in the 289−310 nm range. After doubling, the laser yielded pulse energies of around 1 mJ with a line width of 0.1 cm^{-1}. A 25 cm focal length lens was used to focus the beam at the center of the mass spectrometer. Ions were detected using a microchannel plate that was backed by a phosphor screen (P20). Light emitted by the phosphor was monitored by a photomultiplier. For the recording of mass spectra, the output from the photomultiplier was directed to a digital storage oscilloscope. Mass selected (2+1) REMPI spectra were recorded by using a boxcar integrator to monitor the photomultiplier signals associated with specific ions. Monomer spectra were obtained by detecting HI^+, while complex spectra were recorded by monitoring $ArHI^+$ and/or ArI^+. Very intense (2+1) REMPI signals were observed for HI. Temporal gating of the microchannel plate bias voltage was used to prevent interference resulting from the overloading of the detection system by the HI resonances. A much weaker nonresonant ionization of HI was observed throughout the wavelength range used in this study.

Results

Searches for bands of ArHI were made in the vicinity of the $g^3\Sigma^-(0^+)-X^1\Sigma^+(0^+)$, $d^3\Pi(0^+)-X$, $f\ ^3\Delta_2-X$, and $\Omega = 2-X$ transitions. For the monomer, all of these transitions had been observed previously by (2+1) REMPI.[21] Only one structured band system was found for ArHI. The strongest features of the complex spectrum are shown in Figure 1. This trace was recorded by detecting both $ArHI^+$ and ArI^+ ions. The same spectrum could be obtained by monitoring either ion separately. Figure 2 shows a higher resolution spectrum of the 65 812 cm^{-1} band. Full rotational resolution could not be achieved, but

* Corresponding author. Permanent address: Department of Chemistry, Emory University, Atlanta, GA 30322.

[⊗] Abstract published in *Advance ACS Abstracts,* July 15, 1997.

S1089-5639(97)00784-6 CCC: $14.00

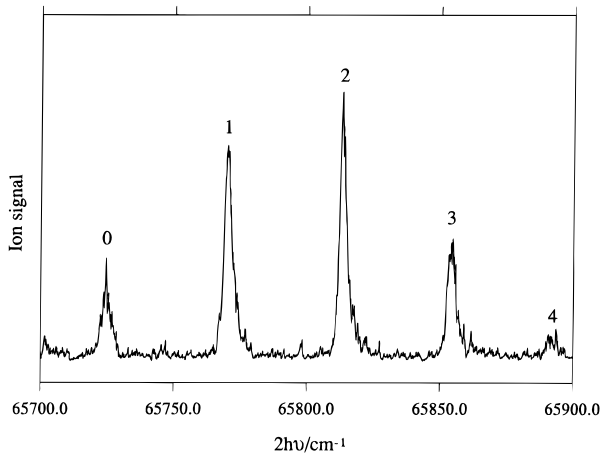

Figure 1. (2+1) REMPI spectrum of the ArHI $g-X$ transition. This trace was obtained by integrating the ion signals for both $ArHI^+$ and ArI^+.

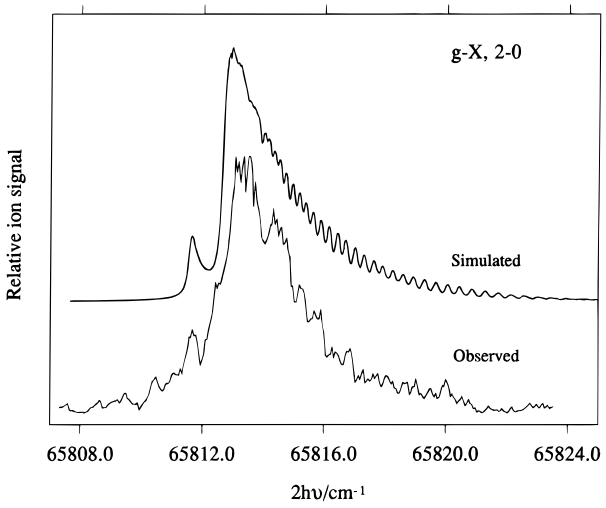

Figure 2. Rotational contours for the ArHI $g-X$ 2−0 band. The lower trace is the observed spectrum. The upper trace is a simulation based on rigid rotor energy levels. The parameters for the simulation were $B'_2 = 0.0392$ cm^{-1}, $B''_0 = 0.0340$cm^{-1}, 0.1 cm^{-1} line width, $T = 20$ K, and $\mu_S^2/\mu_I^1 = 1$. See text for details.

rotational contours were recorded for the stronger bands. Figure 3 shows a mass spectrum obtained with the laser tuned to the center of the 65 812 cm^{-1} band. This trace is typical, in that the $ArHI^+$ and ArI^+ signals are of comparable intensity. There were no discernible signals at the arrival time for Ar_2HI^+ (for all excitation wavelengths), but signals for $(HI)_2^+$ were present. Spectra taken by monitoring the $(HI)_2^+$ ion were featureless for the range of excitation wavelengths used in this study. (2+1) REMPI signals for ArHI were not detected for two-photon energies below 65 720 cm^{-1}. At higher energies weak, nonresonant photoionization of ArHI was observed, extending from about 66 000 cm^{-1} to the highest energy examined (69 200 cm^{-1}). This continuum was detected using a relatively wide boxcar gate, so the ratio of $ArHI^+$ and ArI^+ ions produced was not established. The possibility that HI^+ ions were produced in the process of ionizing ArHI was checked by scanning through the bands shown in Figure 1, while monitoring HI^+. Resonant features were not detected.

Analysis

The spectrum shown in Figure 1 contains a single progression of blue-degraded bands. Band-head positions, determined from the red-edges of the rotational contours, are listed in Table 1.

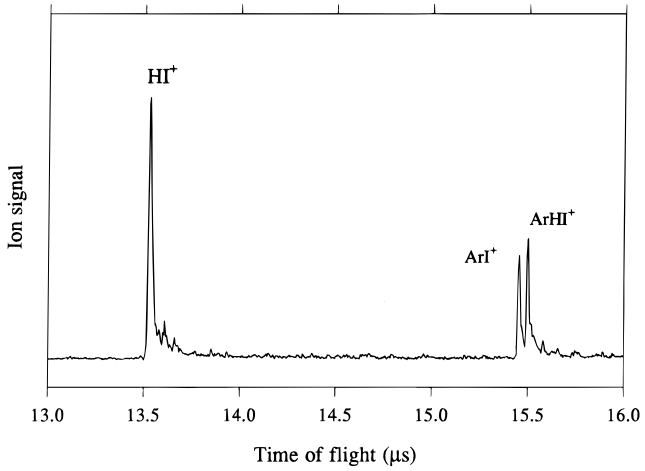

Figure 3. Time-of-flight mass spectrum resulting from (2+1) REMPI of ArHI and weak, nonresonant multiphoton ionization of HI. This trace was recorded with the laser tuned to the maximum of the 2−0 band at 65 812 cm^{-1} ($2h\nu$).

TABLE 1: Band-Head Positions (cm^{-1}) for the $g-X$ Transition of Ar−HI

υ	$\nu_0{}^a$	υ	$\nu_0{}^a$
0	65 722.8	3	65 852.5
1	65 769.1	4	65 890.1
2	65 812.2		

[a] ±0.3 cm^{-1} error limits.

These bands are red-shifted, relative to the HI $g-X$ 0−0 transition by 133−300 cm^{-1}. Their close proximity to this monomer transition, and substantial displacement from any of the other monomer transitions that have been detected by (2+1) REMPI, indicate that the complex bands correlate with $g-X$ 0−0. Further support for this vibronic assignment is provided by a more detailed analysis.

The intervals between the complex bands were consistent with an excited-state progression of the van der Waals stretch mode (υ'_s). The intensity distribution evident in Figure 1 shows that there is a significant change in the intermolecular separation on electronic excitation. For this circumstance the lowest energy band observed is not necessarily the origin band. Consequently, one-dimensional Franck−Condon factor calculations were used to establish the excited-state vibrational numbering. Spectroscopic constants for the g and X states were derived as an integral part of this exercise.

A trial vibrational numbering was assumed, and the band heads were fit to the expression

$$T_{\upsilon_s 0} = T'_{e0} + \omega'_e(\upsilon'_s + {}^1/_2) - \omega_e x'_s(\upsilon'_e + {}^1/_2)^2 \qquad (1)$$

where T'_{e0} is the minimum energy of the effective radial potential (averaged over the monomer stretch and complex bending motions). Note that the quality of this fit (0.8 cm^{-1} standard deviation) was independent of the numbering, as it should be. The dissociation energy, D'_e, and Morse range parameter, β, were then calculated from the vibrational constants using the standard relationships.[22] Franck−Condon factor calculations require some information about the ground state. This was derived from the displacement of the complex spectrum from the monomer parent transition, and an approximate scaling relationship. The ground-state dissociation energy was determined from

$$D''_0 = D'_e - G'(\upsilon_s) + \nu_f - \nu_m \qquad (2)$$

TABLE 2: Molecular Constants and Dissociation Energies for Ar−HI $g^3\Sigma^-(0^+)$[a]

T_{e0}	D_0	D_e	ω_e	$\omega_e x_e$
65 698.7(5)	393(12)	417(12)	49.0(2)	1.44(3)

[a] All constants are in cm^{-1}. Errors in parentheses are 1 standard deviation in the units of the last digit reported.

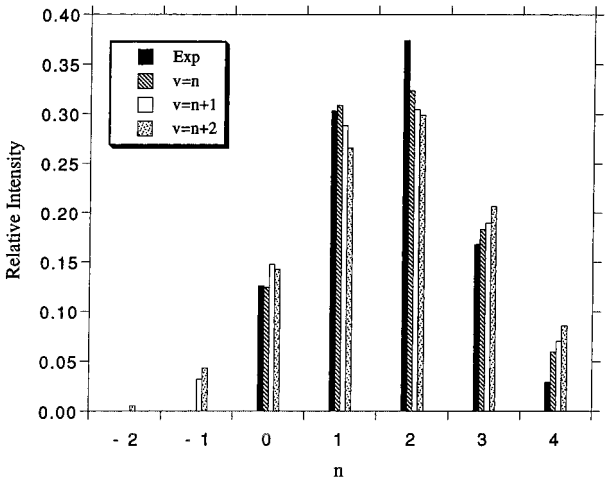

Figure 4. Comparison of observed intensities for the ArHI $g-X$ bands (solid bars) with relative intensities from one-dimensional Franck−Condon factor calculations. The latter were computed for three different trial numberings of the g state vibrational levels. The numbering with $v = n$ corresponds to the labeling of Figure 1.

where ν_f is the energy of the transition to the red-most complex feature (65 722.8 cm^{-1}) and ν_m is the origin of the monomer transition (66 022.6 cm^{-1}).[21] $G'(v_s)$ is the vibrational energy for the red-most feature, with v_s defined by the trial numbering. When Morse energy level expressions are used in eq 2 the ground-state dissociation energy does not depend on the assumed numbering. This treatment yields a dissociation energy of $D''_0 = 93 \pm 12$ cm^{-1}. It is important to note that the error limits given are those resulting from the extrapolation of the Morse parameters (i.e., a Birge−Sponer plot[22]). The ground-state stretch potential was also approximated by a Morse function. The vibrational frequency was estimated from the scaling relationship $\omega''_e \approx \omega'_e D''_0 / D'_0$. Consider, for example, the case where the red-most spectral feature is assigned as the origin band. The g state constants resulting from this assignment are listed in Table 2. These, in turn, yield estimates for the ground-state constants of $\omega'_e = 24$, $\omega_e x''_e = 1.4$, and $D''_e = 105$ cm^{-1}.

Last, for Franck−Condon factor calculations, a value for the difference between the g and X state equilibrium intermolecular separations, $\Delta R_e = R'_e - R''_e$, was needed. As the excited state is more deeply bound than the ground state (regardless of the numbering), and the rotational contours were blue-shaded (cf., Figure 2) it was assumed that ΔR_e is negative. For each trial numbering, Franck−Condon factor calculations were performed for a range of negative ΔR_e values, to find the best match to the intensity distribution seen in Figure 1. The results of these calculations are collected in Figure 4, where the experimental intensities are represented by the solid bars. From this plot it can be seen that the best agreement was obtained by assigning the red-most band as the origin. For this choice the optimum value for ΔR_e was found to be −0.35 Å. Increasing the numbering by one or two units resulted in predictions of bands with observable intensities at energies below the red-most feature, where no bands were evident above the noise level. Furthermore, the intensity distribution of the observed spectrum was rather sharply peaked about the band at 65 812.2 cm^{-1}. None of the calculations fully reproduced this characteristic, but the preferred assignment ($v = n$ in Figure 4) gave the narrowest distribution. Increasing the numbering broadened the distribution because it effectively increased the slope of the attractive limb of the g state in the region of R''_e. At this time we cannot rule out the possibility that the intensities could have been modified by the ionization step or predissociation processes. However, if we assume that these processes were not sensitively dependent on v'_s, the calculations presented here favor the vibrational numbering used in Figure 1 and Table 1. Hence, the g state constants listed in Table 2 represent our current best estimates.

Rotational resolution was not achieved in these measurements, but rotational contours were recorded for several bands. The signal-to-noise ratios of these contours were not good enough to permit independent determination of the rotational constants from a contour analysis. However, they were sufficiently well defined to probe questions of their compatiblity with assignment of the spectrum to HI−Ar and consistency with the ΔR_e value obtained from the Franck−Condon factor calculations. To simulate the contours, estimates for the X and g state rotational constants were needed. For the ground state, data from a high-level ab initio calculation were used to define the constant. In support of these measurements, Yabushita[23] preformed MP4 calculations with cc-pVTZ basis functions for H and Ar, and a relativistic core potential plus cc-pVTZ basis functions for I. These calculations predicted that the minimum energy structure is linear HI(X)−Ar, with a well depth of 140 cm^{-1} and an I−Ar equilibrium distance of 3.97 Å (rotation constant, $B_e'' = 0.035$ cm^{-1}). A secondary minimum was found for linear Ar−HI-(X), lying only 14 cm^{-1} above the global minimum. For this configuration the Ar−H equilibrium distance was 3.04 Å (rotation constant, $B_e = 0.026$ cm^{-1}). The dependence of the rotational constant on v_s was determined using the Pekeris relationship.[22] For the simulations, we assumed that the transitions originated from the zero-point level located near the HI−Ar minimum ($B_0'' = 0.0340$ cm^{-1}). On excitation to the g state the equilibrium intermolecular distance contracts by 0.35 Å, yielding an excited equilibrium rotational constant of $B_e' = 0.0417$ cm^{-1}. This result, combined with the estimate for α_e from the Pekeris relationship, gives $B_v' = 0.0417 - 0.001(v_s + {}^1/_2)$. Rotational contours were simulated using linear rigid-rotor energy levels, a Boltzmann population distribution, a laser line width of 0.1 cm^{-1}, and the two-photon rotational line-strength factors for a linear molecule $\Omega' = 0 - \Omega'' = 0$ transition.[24] For the latter, Bray and Hochstrasser[24] derived the expressions:

O-branch $$S_{J-2\leftarrow J} = \frac{J(J-1)}{30(2J-1)}{\mu_S}^2$$

S-branch $$S_{J+2\leftarrow J} = \frac{(J+1)(J+2)}{30(2J+3)}{\mu_S}^2$$

Q-branch $$S_{J\leftarrow J} = \frac{(2J+1)}{9}{\mu_I}^2 + \frac{J(J+1)(2J+1)}{45(2J-1)(2J+3)}{\mu_S}^2$$

where μ_S^2 and μ_I^2 are transition moment dipole factors. Only two parameters were varied to fit the observed contours. These were the temperature and the ratio μ_S^2/μ_I^2. Figure 2 shows a simulation of the 2−0 band with $T = 20$ K and $\mu_S^2/\mu_I^2 = 1$. The contours were not very sensitive to the transition dipole ratio, and values in the range 0.7−1.3 gave reasonable results. Figure 2 shows that the rotational contours were clearly consistent with assignment of the spectrum to HIAr and the foregoing analysis of the intensity distribution.

Discussion

Excitation of the ArHI $g-X$ transition is accompanied by an increase in the strength of the intermolecular interaction and a decrease in the van der Waals bond length. Similar behavior on electronic excitation has been noted for other Ar−hydride complexes (e.g., OH−Ar,[25,26] SH−Ar,[27] BH−Ar[28]). One obvious factor involved in these changes is the greater polarizability of the monomer in an electronically excited state. As the g state is a Rydberg state, it should be very polarizable.

The dissociation energy for HI(X) estimated from the (2+1) REMPI spectrum ($D_0'' \approx 93$ cm^{-1}) is consistent with Yabushita's[23] ab initio value of $D_e'' = 140$ cm^{-1}. This result is also comparable to the dissociation energies of ArHF ($D_0'' = 101.3$ cm^{-1}),[9] ArHCl ($D_0'' = 114.7$ cm^{-1}),[1,7] and ArHBr ($D_0'' = 121.2$ cm^{-1}).[1,8] The ArHI(X) dissociation energy does not appear to fit the trend of increasing bond strength with increasing mass of the halogen atom. However, this anomaly may be no more than an artifact of the assumptions made in the analysis. Birge−Sponer extrapolations often underestimate dissociation energies (particularly when van der Waals forces are involved, which have greater range than the exponentially decreasing forces of the Morse potential).[22] In contrast to ArHF, ArHCl, and ArHBr, the calculations for HI−Ar favor bonding of the Ar atom to the heavy (and very polarizable) I atom. This is consistent with the trends noted by Hutson[1]. The energy difference between the minima for Ar−HX and HX−Ar decreases from 85 cm^{-1} for ArHF to 5 cm^{-1} for ArHBr. Extrapolation of this trend suggests that HI−Ar will be the more stable isomer. Segall et al.[15] reported indirect evidence for this structure. They did not see "slow" hydrogen atoms when the products from an expansion of HI in Ar were photolyzed. The absence of this signature of trapped trajectories was attributed to the unfavorable HI−Ar geometry. Unfortunately, we were unable to determine the equilibrium geometry of HI(X)Ar from the spectrum. Final confirmation of the structure must await higher resolution spectroscopic studies of ArHI and ArDI.

Regardless of the equilibrium geometry, ArHI is not a good candidate for studies of the one-atom cage effect. The weakness of the van der Waals bond virtually guarantees that it will execute large-amplitude bending. Schröder et al.[17] have shown that zero-point bending motion can effectively evade trapped trajectories when the amplitude is large (e.g., the zero-point motions of Ar−HCl, Ar−HBr, and ArHI).

Bands corresponding to excitation of the bending mode of ArHI were not seen in the $g-X$ spectrum. This result is easily explained in terms of vibrational wave function overlap, if the barrier to internal rotation changes substantially on electronic excitation. As the radial well-depth increases by a factor of 4, it is not surprising to find that the change in the anisotropy is sufficient to effectively suppress observation of the bending bands. (Similar behavior has been observed in the $A-X$ transition of OH−Ar, where excited bending levels can be seen only in combination with stretch levels at energies near the dissociation limit[29]).

Resonant ionization of ArHI produced both $ArHI^+$ and ArI^+ ions, and it is of interest to speculate on the origin of the latter. The wavelengths used to access the $g-X$ transition can also cause single photon dissociation of HI. In their study of HI, Wright and McDonald[21] detected REMPI signals from I($^2P_{3/2}$) atoms that originated from single-photon dissociation (i.e., HI + hν → H + I followed by I + 3$h\nu$ → $I^+ + e^-$). Two observations of the present work exclude the possibility that the ArI^+ fragment ions resulted from a single-photon dissociation process: The spectrum shown in Figure 1 could be obtained by monitoring ArI^+, and the fragment ion was not generated when the laser was off-resonance. Breaking of the H−I bond could occur before or after the absorption of a third photon. Examples of such processes include

$$\mathrm{ArHI} + 2h\nu \rightarrow \mathrm{ArHI}(g); \qquad \mathrm{ArHI}(g) + h\nu \rightarrow \mathrm{ArHI}^+{}^*; \quad \mathrm{ArHI}^+{}^* \rightarrow \mathrm{ArI}^+ + \mathrm{H}$$

$$\mathrm{ArHI} + 2h\nu \rightarrow \mathrm{ArHI}(g); \qquad \mathrm{ArHI}(g) \rightarrow \mathrm{ArI}(^2\mathrm{P}) + \mathrm{H}; \quad \mathrm{ArI}(^2\mathrm{P}) + 2h\nu \rightarrow \mathrm{ArI}^+$$

where the asterisk denotes internal excitation. The present measurements could not determine how many photons were absorbed prior to fragmentation. The fact that ArHI does fragment at some stage of the ionization process is interesting, given that (2+n) REMPI of HI via the g state does not produce I^+ fragments.[21] Hence, for ArHI or $ArHI^+$ to fragment, the mechanism must involve predissociation of an excited state of HI or HI^+ induced by the presence of the nearby Ar atom. Rapid electronic predissociations of the two-photon excited states of ArHI (other than the g state) could explain why we were unable to find structured bands for the states lying above the g state.

Conclusion

ArHI was detected by spectroscopic means for the first time. A vibrationally resolved (2+1) REMPI spectrum was recorded for the $g^3\Sigma^-(0^+)-X^1\Sigma^+(0^+)$ transition. Analysis of these data yielded stretching vibrational constants for the g state and estimates for the van der Waals bond strengths in the g and X states. The ground state is weakly bound, and ab initio calculations predict a linear HI−Ar geometry. These properties indicate that ArHI is a poor candidate for studies of the cage effect. As it is likely that the heavier rare-gas atoms will also bind to the iodine atom, the other HI−Rg complexes may also be unsuitable. Schröder et al.[17] have argued that ArHCl (and, by implication, ArHBr) will not be suitable for cage effect studies due to large-amplitude bending. KrHX and XeHX (X = Cl or Br) complexes may be more favorable, as they have greater barriers to internal rotation. Further reduction in the bending amplitude could be achieved by deuteration. The (2+1) REMPI detection technique demonstrated here for ArHI should be applicable to KrDX and XeDX complexes.

Acknowledgment. We thank Professor S. Yabushita (Keio University) for making the results of his ab initio calculations on ArHI available prior to publication. M.C.H. thanks Professor T. Suzuki and the Institute for Molecular Science for sponsoring his sabbatical visit. This work was funded by a Grant-in-Aid on Priority-Area-Research "Small Many-Body Systems" from the Ministry of Education, Science, Sports, and Culture, and the National Science Foundation (CHE-9320094).

References and Notes

(1) Hutson, J. M. *Annu. Rev. Phys. Chem.* **1990**, *41*, 123.
(2) Cohen, R. C.; Saykally, R. J. *J. Phys. Chem.* **1992**, *96*, 1024.
(3) Nesbitt, D. J. *Chem. Rev.* **1988**, *88*, 843.
(4) Miller, R. E. *Adv. Mol. Vibr. Collision Dyn.* **1991**, *1*, 83.
(5) Chang, H.-C.; Klemperer, W. *Faraday Discuss.* **1994**, *97*, 95.
(6) Nesbitt, D. J.; Child, M. S.; Clary, D. C. *J. Chem. Phys.* **1989**, *90*, 4855.
(7) Huston, J. M. *J. Chem. Phys.* **1988**, *89*, 4550.
(8) Hutson, J. M. *J. Chem. Phys.* **1989**,*91*, 4455.
(9) Hutson, J. M. *J. Chem. Phys.* **1992**, *96*, 6752.
(10) Jackson, K. C.; Langridge-Smith, P. R. R.; Howard, B. J. *Mol. Phys.* **1980**, *39*, 817.
(11) Firth, D. W.; Dvorak, M. A.; Reeve, S. W.; Ford, R. S.; Leopold, K. R. *Chem. Phys. Lett.* **1990**, *168*, 161.
(12) Alimi, R.; Gerber, R. B. *Phys. Rev. Lett.* **1990**, *64*, 1453.

(13) Garcia-Vela, A.; Gerber, R. B. *J. Chem. Phys.* **1993**, *98*, 427.
(14) Garcia-Vela, A.; Gerber, R. B.; Imre, D. G.; Valentini, J. J. *Phys. Rev. Lett.* **1993**, *71*, 931.
(15) Segall, J.; Wen, Y.; Singer, R.; Wittig, C.; Garcia-Vela, A.; Gerber, R. B. *Chem. Phys. Lett.* **1993**, *207*, 504.
(16) Garcia-Vela, A.; Gerber, R. B.; Imre, D. G.; Valentini, J. J. *Chem. Phys. Lett.* **1993**, *202*, 473.
(17) Schröder, T.; Schinke, R.; Mandziuk, M.; Bacic, Z. *J. Chem. Phys.* **1994**, *100*, 7239.
(18) Suzuki, T.; Ito, M. *J. Phys. Chem.* **1987**, *91*, 3537.
(19) Callaghan, R.; Arepalli, S.; Gordan, R. J. *J. Chem. Phys.* **1987**, *86*, 5273.
(20) Callaghan, R.; Gordon, R. J. *J. Chem. Phys.* **1990**, *93*, 4624.
(21) Wright, S. A.; McDonald, J. D. *J. Chem. Phys.* **1994**, *101*, 238.
(22) Herzberg, G. *Molecular Spectra and Molecular Structure. I. Spectra of Diatomic Molecules*; Van Nostrand Reinhold: New York, 1950.
(23) Yabushita, S., private communication.
(24) Bray, R. G.; Hochstrasser, R. M. *Mol. Phys.* **1976**, *31*, 1199.
(25) Fawzy, W. M.; Heaven, M. C. *J. Chem. Phys.* **1988**, *89*, 7030; **1990**, *92*, 909.
(26) Berry, M. T.; Brustien, M. R.; Adamo, J. R.; Lester, M. I. *J. Phys. Chem.* **1988**, *92*, 2,
(27) Yang, M.-C.; Salzberg, A. P.; Chang, B.-C.; Carter, C. C.; Miller, T. A. *J. Chem. Phys.* **1993**, *98*, 4301.
(28) Alexander, M. H.; Gregurick, S.; Dagdigian, P. J. *J. Chem. Phys.* **1994**, *101*, 2887.
(29) Bowman, J. M.; Gazdy, B.; Schafer, P.; Heaven, M. C. *J. Phys. Chem.* **1990**, *94*, 2226.